Cross-section behaviour of cold-formed high strength steel irregular hexagonal hollow section stub columns under combined compression and bending

Jun-zhi Liu[1]; Tak-Ming Chan[2,3 *]; Ben Young[2]

[1] School of National Safety and Emergency Management, Beijing Normal University, China.

[2] Department of Civil and Environmental Engineering, The Hong Kong Polytechnic University, Hong Kong, China

[3] Chinese National Engineering Research Centre for Steel Construction (Hong Kong Branch), The Hong Kong Polytechnic University, Hong Kong, China

* Corresponding author: tak-ming.chan@polyu.edu.hk

Abstract

Cross-section behaviour for cold-formed high strength steel (HSS) irregular hexagonal hollow section (IHexHS) stub columns under combined compression and bending is studied and presented in this paper. Finite element models were developed and validated using the existing experimental data collated from the previous research. Upon the validated finite element models, extensive parametric studies were subsequently carried out to generate more numerical data covering a wider range of cross-section dimensions, steel grades and load combinations from pure compression to pure bending. The obtained numerical results were utilised to assess the accuracy and the applicability of the current design codes, such as Eurocode of EN 1993-1-12 (EC3) and the North American code of ANSI/AISC 360-16 (AISC) for cold-formed HSS IHexHS stub columns under combined loading. It was demonstrated that the existing design codes can be safely applied and can be extended for cold-formed HSS IHexHS stub columns design under combined loading. In cross-sectional resistance predictions, conservative results were provided from the existing design codes. The over-predictions were primarily due to the neglect of the strain hardening and plate element interaction. The end points used in the interaction curves of EC3 and AISC adopt an idealised elastic-plastic material model to derive the corresponding resistance in cross-sectional level. The employment of Continuous Strength Method (CSM) leads to improved accuracy in cross-sectional resistance prediction with updated end points in the interaction curve. More consistent and reliable predictions were revealed by carrying out reliability analysis in accordance with EN 1990.

Keywords: cross-section behaviour; Irregular hexagonal hollow sections; High strength steel; Material properties; Design methods.

1. Introduction

Steel tubular structural members are widely adopted in the construction industry including buildings, bridges and offshore structures because of the appealing appearance and prominent performance in resisting the buckling loads (Chan and Gardner 2008; Ma et al. 2015; Liu et al. 2022a). The family of tubular members typically comprise conventional profiles of rectangular- (RHS), square- (SHS), circular- (CHS) and elliptical hollow sections (EHS). With the advancement in production technology and welding techniques, tubular sections in different cross-section configurations with combined structural efficiency and architectural aesthetics have attracted increasing interests from the researchers. Cold-formed steel oval hollow sections have been investigated by Zhu and Young (2011) and cold-formed semi-oval hollow sections have been studied by Chen and Young (2019, 2020). In recent years, increasing interests have also been made focusing on the applications of polygonal sections such as high strength steel (HSS) hexagonal-(HexHS), irregular hexagonal- (IHexHS), octagonal- (OctHS) and irregular octagonal hollow sections (IOctHS). The advantages of using HexHS/IHexHS and OctHS/IOctHS have been illustrated that the width of the flat portion is smaller than counterparts of square and rectangular hollow sections (SHS/RHS) if they are delivered with similar perimeters, therefore exhibiting stronger local buckling resistance than that of SHS and RHS (Liu et al. 2022g, 2022h). In addition, the flat surfaces allow for easier construction by providing an operating platform for welding or bolt-connection with end plate or gusset plate.

Experimental investigations on material properties and residual stresses for high strength steel (HSS) HexHS/IHexHS have been conducted by Liu et al. (2022a, 2022b) with sections made of Q690 steel grade (nominal yield strength f_y = 690 MPa). Material properties and residual stresses investigations of OctHS/IOctHS have been experimentally studied by Zhu et al. (2019) with sections made of conventional mild steel with nominal yield strength of 355 MPa, and by Fang et al. (2018) and Liu et al. (2022c) with sections comprising Q690 steel plates with nominal yield strength of 690 MPa, and by Chen et al. (2020) with specimens made of Q460 steel plates with nominal yield strength of 460 MPa. In addition, local buckling behaviour of the HSS HexHS/IHexHS and OctHS/IOctHS stub columns under concentric compression have also been studied. The applicability of the existing structural steel design codes of EN 1993-1-1 (CEN 2005), EN 1993-1-5 (CEN 2004), EN 1993-1-12 (CEN 2007), AISI/AISC 360-16 (AISC 2016) and AS 4100 (AS 2020) have been evaluated and compared. The previous studies demonstrated that the cross-section classification slenderness limit value cannot simply be extended to classify the cross-

section of HexHS/IHexHS and OctHS/IOctHS under pure compression. The design equations in terms cross-sectional resistance under pure compression also exhibit either over-conservatism for stocky sections or unsafe predictions for sections subject to local buckling prior to the attainment of cross-section yielding. Despite the illustrative prominent advantages of HexHS/IHexHS and OctHS/IOctHS, limited studies have been carried out which further need to be systematically explored. Existing studies for cold-formed HSS IHexHS have been performed to study material properties, residual stresses and its structural behaviour at cross-sectional level under concentric compression. To better understand the structural behaviour and promote the application of HSS IHexHS, investigations of local buckling performance under combined compression and bending should be carried out.

Conventional tubular profiles of RHS/SHS and CHS with high strength steel materials are codified in current design codes of EN 1993-1-12, AISI/AISC 360-16. Note that provisions of high strength steel sections with nominal yield strength 690 MPa have been provided in AISI/AISC 360-16 (AISC 2016), and EN 1993-1-12 (CEN 2007) which extend the design framework for mild steels in EN 1993-1-1 (CEN 2005) to high strength steel with strength grade up to steel grade of S700. Nevertheless, stringent requirements are proposed to tubular sections in AISI/AISC 360-16. AISI/AISC 360-16 specifies that hollow sections with nominal yield strength not greater than 485 MPa are only allowed to be designed. Whether the current structural steel design codes can be extended to cover the design of HSS IHexHS stub columns under combined compression and bending is unknown. The applicability of the existing design codes to the HSS HexHS stub columns needs to be assessed and evaluated.

Moreover, the design approach of Continuous Strength Method (CSM), which can rationally exploit the effects of strain hardening and redistribution of plasticity, was also evaluated and assessed for extending the application scope covering cold-formed HSS IHexHS stub columns under combined compression and bending. This paper therefore presents numerical investigation on cross-section behaviour of cold-formed HSS IHexHS stub columns under combined loading. The finite element models were firstly developed and validated against existing test results collated from cold-formed HSS SHS/RHS sections under combined compression and bending (Ma et al. 2019) and cold-formed HSS OctHS under combined loading (Fang et al. 2021). The validated finite element models were subsequently employed to conduct extensive parametric studies, covering a wider range of loading combinations and steel grades of Q460 and Q690. The obtained

ultimate resistances from parametric studies were used to assess the applicability and accuracy of the current design codes and design approach of CSM.

2. Numerical investigation

2.1 General

A comprehensive numerical modelling programme was conducted including the development of the finite element models (FEM), validation and parametric studies. The FEM was developed using the software package of ABAQUS (ABAQUS 2014). The adopted notations for the geometries of the cold-formed HSS IHexHS stub column are illustrated in Fig. 1, where H is the height of the cross section, B is the outer width of the IHexHS, B_L is the longer edge length of the IHexHS, b_L is the clear width of the vertical flat portion with welding bead excluding the corner regions, B_s is the shorter edge length, b_s is the clear width of an inclined short flat side excluding the corner portions, t is the nominal thickness of the cross section, r_o and r_i are the outer and inner corner radius of the cross section respectively, $e_{0,y}$ and $e_{0,z}$ are the initial eccentricity magnitudes around the major and minor axis respectively. The FEM was firstly validated against the existing test results of HSS cold-formed SHS and RHS in Ma et al. (2019) and Fang et al. (2021). Subsequently, extensive parametric studies were carried out to generate additional structural performance data on cold-formed HSS IHexHS stub columns under combined loadings.

2.2 Development of finite element model

The four-noded shell element with reduced integration (S4R) was employed in modelling cross-sections, which have successfully applied in modelling shell elements (Chan et al. 2015; Liu et al. 2022e, 2022f, 2023). Based on the preliminary mesh sensitivity studies, mesh size with a uniform value of $b_s/20$ was adopted for the flat portions of the modelled specimens and a finer mesh of $b_s/30$ was assigned to the corner portions to explicitly account for the curved geometry. To accurately represent the structural behaviours of the modelled specimens, measured geometries and experimentally tested engineering stress-strain relationships were used. The measured stress-strain curves were converted to the true stress-plastic strain curves in accordance with Eqs. (1)-(2). Plastic material model with isotropic hardening was used for modelling steel materials.

$$\sigma_{\text{true}} = \sigma_{\text{eng}}(1+\varepsilon_{\text{eng}}) \quad (1)$$

$$\varepsilon_{\text{true}}^{\text{pl}} = \ln(1+\varepsilon_{\text{eng}}) - (\frac{\sigma_{\text{true}}}{E_{\text{s}}}) \quad (2)$$

where σ_{eng} and ε_{eng} are the engineering stress and engineering strain from tensile coupon tests, E_{s} is Young's modulus obtained from the tests, and σ_{true} and $\varepsilon_{\text{true}}^{\text{pl}}$ are the true stress and plastic strain.

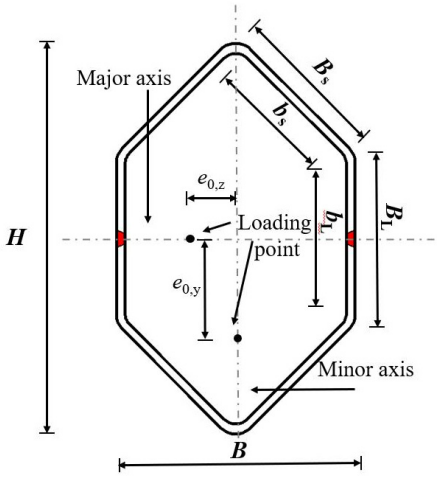

Fig. 1. Definition of symbols for HSS irregular hexagonal hollow section.

To explicitly account for the effects of the cold-forming fabrication process, the enhanced material strengths were incorporated into the corner portions. Moreover, it was found that the enhancement of the strength was not limited to the corner portion only, observations have been made that strength increase can be extended to a certain distance away from the corner portion.

It was found that extension of the corner strength to adjacent flat portions with a magnitude of $2t$ achieve the best agreement between the numerical models and the experimental results for HSS cold-formed SHS/RHS in Ma et al. (2016). As for the cold-formed HSS IHexHS specimens examined in this study, no corner extension was needed basing on the preliminary sensitivity study of extension of cold-forming effect.

Table 1 Summary of the tensile coupon test results.

Specimen	References	Steel grade	Flat coupon						Corner coupon				
			t	E	f_y	f_u	ε_f	ε_u	E_c	$f_{y,c}$	$f_{u,c}$	$\varepsilon_{f,c}$	$\varepsilon_{u,c}$
			(mm)	(N/mm^2)	(N/mm^2)	(N/mm^2)	(%)	(%)	(N/mm2	(N/mm^2)	(N/mm^2)	(%)	(%)
OHS-50×6	Fang et al. (2021)	S690	6	213000	756	800	13.6	4.6	215000	780	850	11.3	1.9
OHS-70×6		S690	6	215000	760	801	14	4.4	196000	785	840	11.3	1.2
H120×120×4	Ma et al. (2019)	H-series	4	212000	689	813	17	5.7	217000	923	996	10	1.7
V80×80×4		V-series	4	21000	1005	1187	18	5.5	208000	1187	1299	10	1.8

Linear elastic buckling analysis was performed to obtain the lowest elastic buckling eigen mode under the combined compression and bending, which was taken as the representative distributed profile of initial local geometric imperfection. The measured imperfection magnitudes were used and scaled to the corresponding profile from linear perturbation. For the modelled cold-formed HSS IHexHS stub columns, the imperfection measurement results were extensively analysed in Liu et al. (2022d) with predictive model of the initial local geometric imperfection (ω_{pred}) proposed, as given in Eq. (3).

$$\omega_{pred} = 0.09t\left(\frac{f_y}{f_{cr}}\right)^{0.5} \quad (3)$$

where f_{cr} is the elastic local buckling stress for the plate with the largest slenderness in a cross section, and f_y is the measured yield strength of the parent plate.

To simulate the pin-ended boundary conditions for eccentrically loaded stub column specimens, the displacement-controlled loads were applied to the reference points locating at the centroid of the modelled specimens, offsetting from the corresponding end sections at a distance equal to the sum of the thickness of the knife edge, end plate and wedge plate in longitudinal direction. The initial eccentricities were incorporated into the FE models by subsequently offsetting the reference points from the centroid of the end section to the measured values in the tests in the direction perpendicular to the bending axis. The reference points were constrained to the nodes at the edges of the end sections through kinematic coupling constraints. The reference points were restrained against all other degree of freedoms, except for the longitudinal displacements at the loading point and the rotation around the bending axis to simulate the pin-ended boundary conditions. The compressive load was applied by specifying the axial displacement of the reference point at one end with nonlinear geometric parameter activated to allow for large displacement analysis. Typical loading and boundary conditions of the cold-formed HSS IHexHS stub columns under combined compression and bending are shown in Fig. 2.

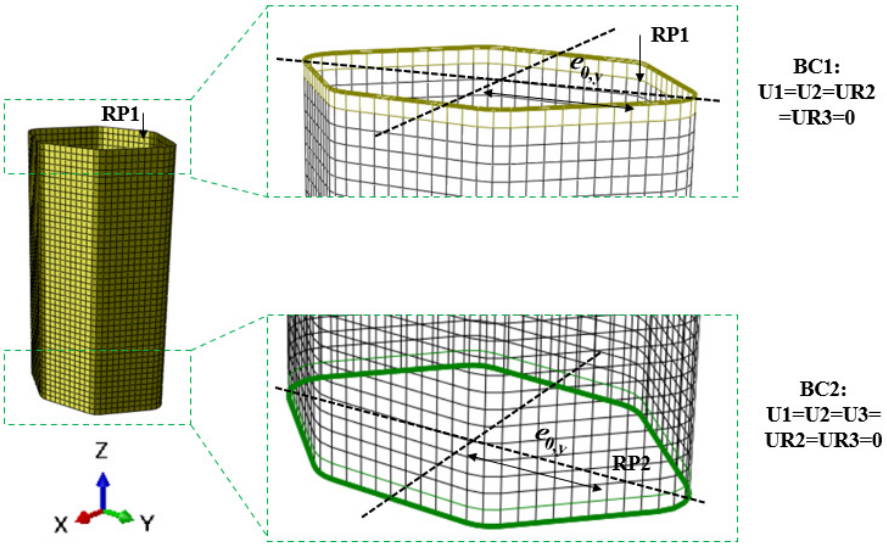

174
175

176 **Fig. 2.** Typical loading and boundary conditions of the HSS IHexHS stub columns under combined
177 compression and bending.

178
179

180 The fabrication processes of cold-forming and welding generate inter-locked existing residual stresses in an
181 unloaded state. The residual stresses can be decomposed into membrane residual stresses and bending
182 residual stresses. It is known that the bending residual stresses are considered to be inherently reintroduced
183 to the stress-strain curves during tensile coupon tests in straightening the curved coupon specimen (Liu et al.
184 2022g). The effect of the residual stress on the structural performance were therefore considered by
185 incorporating the membrane residual stresses with magnitudes determined from predictive model of residual
186 stress distribution provided by Ma et al. (2015) for cold-formed HSS SHS/RHS and by Fang et al. (2018)
187 for HSS cod-formed OctHS and by Liu et al. (2022b) for cold-formed HSS IHexHS.

188

189 2.3 Validation

190

191 The accuracy of the developed FE modes was validated by comparing the numerical test results in terms of
192 failure modes, load-end rotation relationships and ultimate resistances with those obtained from the
193 experimental tests. A total of 6 eccentrically loaded HSS cold-formed SHS/RHS stub columns with sections
194 made from H-series steel (nominal yield strength f_y = 700 MPa) and V-series steel (nominal yield strength =
195 900 MPa) and 8 HSS cold-formed OctHS stub columns with sections made from S690 steel (nominal yield

strength = 690 MPa) were used for the validations of the FF models. The measured material properties of the modelled specimens are shown in Table 1. Figs 3–4 plot the comparisons between the experimental and numerical load-end rotation curves of the representative modelled specimens of HSS cold-formed SHS/RHS and OctHS with various initial eccentricity values. The experimental load-end rotation responses can be accurately captured by the developed FE models. In addition, the failure modes from FE models were compared with experimentally failed specimens as shown in Fig 5 for cold-formed HSS SHS stub column specimen of H120×120×4-e30 and Fig 6 for cold-formed HSS OctHS stub column specimen of OHS-70×6-e75. Table 2 reports and summarises the comparisons between the experimental and numerical results of cross-sectional resistance for cold-formed HSS SHS and OctHS stub columns under combined loading. The average values of the ratios of $P_{u,test}/P_{u,FE}$ are 1.01 and 1.01 for HSS cold-formed SHS and OctHS with the coefficient of variation values (CoV) of 0.03 and 0.01 respectively. Overall, the developed FE models can successfully replicate the failure modes and accurately predict the ultimate resistance of the eccentric stub columns with satisfactory agreements in load-end rotation responses.

Table 2 Comparison of the experimental and numerical results.

References	Steel grade	Specimen	$P_{u,test}$ (kN)	$P_{u,FE}$ (kN)	$P_{u,test}/P_{u,FE}$
Ma et al. (2019)	H-series	H120×120×4-e5	1200	1208.5	0.99
		H120×120×4-e30	788	793.6	0.99
		H120×120×4-e60	576	589.6	0.98
		H120×120×4-e120	366	359.5	1.02
	V-series	V80×80×4-e20	794	782.2	1.02
		V80×80×4-e80	346	325.4	1.06
				Mean	1.01
				Cov	0.03
Fang et al. (2021)	S690	OHS-50×6-e25	1177.1	1181.8	0.99
		OHS-50×6-e50	843.2	832.4	1.01
		OHS-50×6-e100	524.4	517.8	1.01
		OHS-50×6-e125	426.3	412.2	1.03
		OHS-70×6-e25	1818.3	1796.7	1.01
		OHS-70×6-e50	1441.7	1421.8	1.01
		OHS-70×6-e75	1111.2	1119.0	0.99
		OHS-70×6-e100	912.7	896.8	1.02
				Mean	1.01
				CoV	0.01

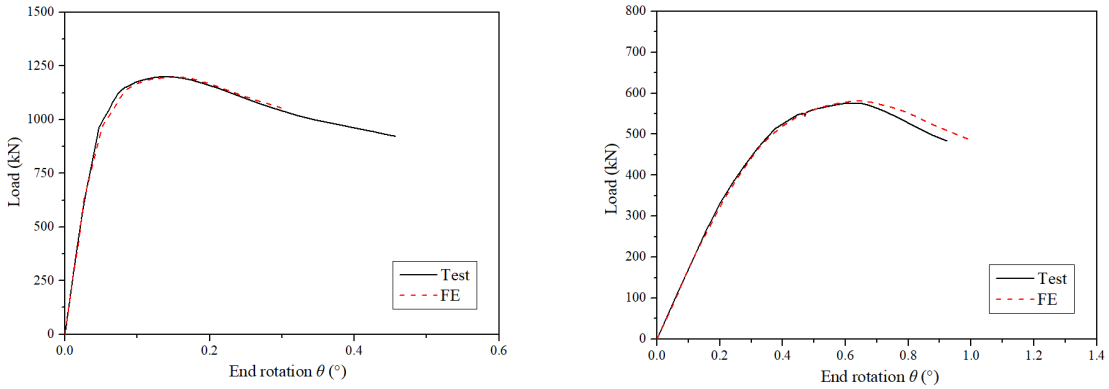

(a) H120×120×4-e5 (b) H120×120×4-e60

Fig. 3. Comparisons between experimental and numerical load-end rotation curves for cold-formed SHS stub columns under combined loading (Ma et al. 2019).

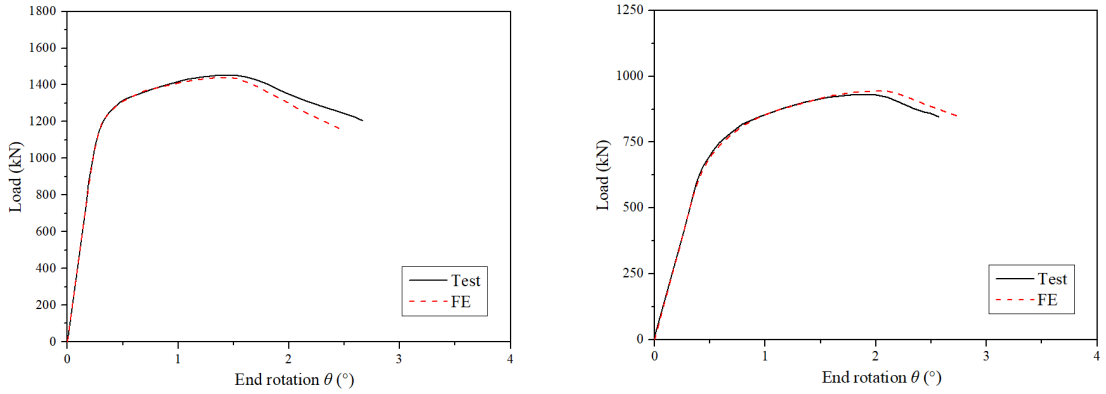

(a) OHS-70-6-e50 (b) OHS-70-6-e100

Fig. 4. Comparisons between experimental and numerical load-end rotation curves for cold-formed octagonal stub columns under combined loading (Fang et al. 2021).

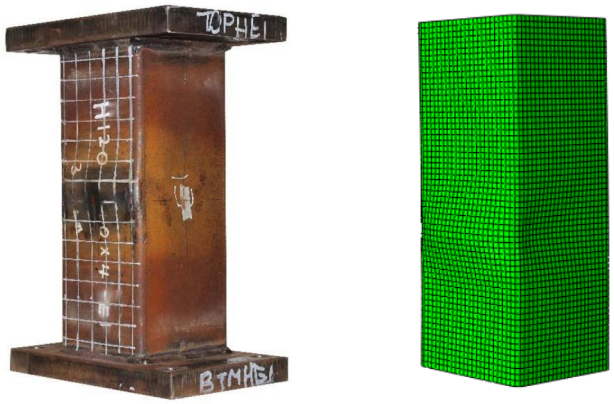

Fig. 5. Comparison of typical failure mode from experimental test and numerical simulation for cold-formed SHS stub column of H120×120×4-e30 (Ma et al. 2019).

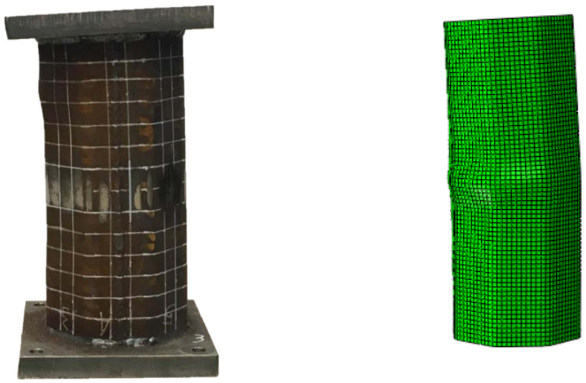

Fig. 6. Comparison of typical failure modes from experimental test and numerical simulation for cold-formed octagonal hollow section stub column of OHS-70×6-e75 (Fang et al. 2019).

2.4 Parametric study

Following the validation of the FE models, an extensive parametric study on cold-formed HSS IHexHS stub columns under combined compression and bending was carried out with varying cross-sectional slenderness and a wider range of combinations of compression and bending as well as loading conditions including compression plus both major and minor axis bending. Full stress-strain curves up to f_u for steel materials Q460 and Q690 with nominal yield strength of 460 MPa and 690 MPa measured in Chen et al. (2020) and Liu et al. (2022b) were used and generated using the respective proposed predictive models respectively. The average material properties were used with the key material properties adopted in parametric study for both flat and corner portions reported in Table 3, including the Young's modulus E_s, the yield strength f_y, the ultimate strength f_u, and the ultimate strain ε_u. The subscripts of "f" and "c" denote the flat and corner portions of the cross-sections. The stress-strain curves of the cold-formed HSS employed in parametric studies are plotted in Fig. 7 for both flat and corner portions respectively.

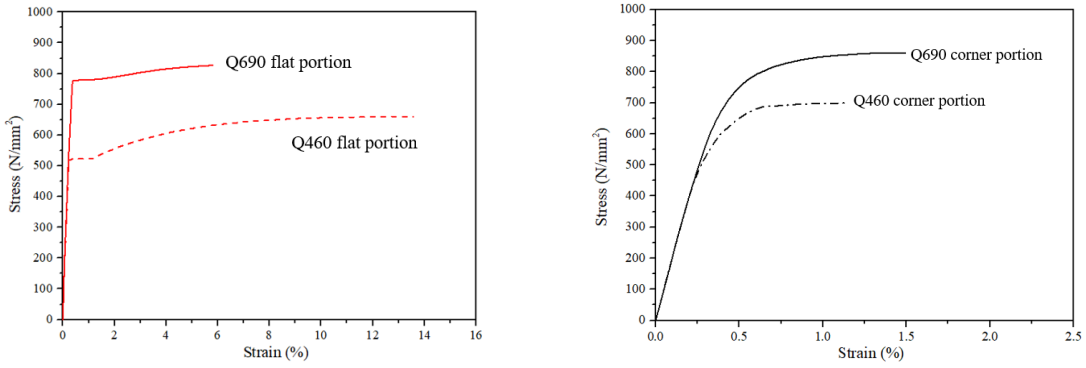

(a) (b)

Fig. 7. Stress-strain curves of cold-formed HSS IHexHS stub columns employed in parametric study (a) Stress-strain curves of flat portions (b) Stress-strain curves of corner portions.

The initial local geometric imperfection was incorporated in the FE model by scaling the predicted imperfection magnitude to the lowest elastic buckling mode. The membrane residual stresses were included in the FE models using the simplified predictive model of residual stress distribution for cold-formed HSS IHexHS provided in Liu et al. (2022b), as shown in Fig. 8.

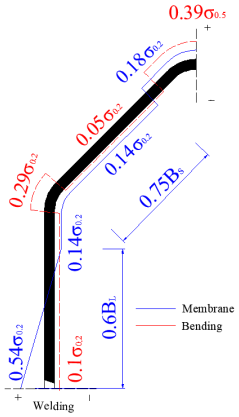

Fig. 8. Predictive model of membrane and bending residual stresses distribution and amplitudes in FE modelling (Liu et al. 2022b).

Table 3 Key material properties adopted in parametric study.

	Flat portion				Corner portion			
Steel grade	E_s (N/mm^2)	f_y (N/mm^2)	f_u (N/mm^2)	ε_u (%)	$E_{s,c}$ (N/mm^2)	$f_{y,c}$ (N/mm^2)	$f_{u,c}$ (N/mm^2)	$\varepsilon_{u,c}$ (%)
Q690 (Liu et al. 2022b)	210000	770	825	6.5	200000	815	845	1.75
Q460 (Chen et al. 2020)	213900	581	669	11.7	198200	735	776	1.33

The length of all the specimens were designed as 2.5 times the average cross-section dimensions, which are short enough to avoid interaction effect from global buckling but sufficiently long to contain the representative initial local geometric imperfection and residual stresses. The thickness of the modelled IHexHS was kept constant as 6 mm, and the inner corner radius of the cold-bent corner of each specimen r_i was taken equal to three times of its thickness. The effect of the cross-section slenderness was investigated by varying the lengths of the clear width of the vertical flat portion b_L and the clear width of an inclined short flat side excluding the corner portions b_s. The cold-formed HSS IHexHS is a novel cross-section which

is not covered in existing design codes for traditional profile. Thus, cross-sectional slenderness parameter of $\lambda_p = (f_{cr}/f_y)^{0.5}$ was used, where f_{cr} is the elastic buckling stress of the cross-section under the applied loading conditions, which can be derived using finite strip software of CUFSM or ABAQUS, and f_y is the measured yield strength from the flat portion. The cross-section slenderness of the numerical models for parameter studies were within the range of $\lambda_p \leq 0.64$, based on the experimental investigation on cross-section classification of cold-formed HSS IHexHS in Liu et al. (2022d). Furthermore, the slenderness limit value of $\lambda_p = 0.68$ is specified as the boundary between slender and non-slender sections for CSM, the numerical results from parametric studies were thereof within the application range of CSM for non-slender sections. The load eccentricities were designed to yield a wider spectrum of compression and bending combinations. The ratios of the compression load to bending was represented using a dimensionless parameter, defined as radial angle θ, as illustrated in Fig. 9. This dimensionless parameter can be derived as per Eq. (4), where P_{Rd} and M_{Rd} are the design resistances for stub column specimens under pure compression and pure bending respectively, and P_{Ed} and M_{Ed} are the design compression load and bending moment respectively. Based on the definition of the radial angle θ, the pure compression case can be expressed as $\theta = 0°$ whereas the pure bending scenario can be expressed as $\theta = 90°$.

$$\theta = \tan^{-1}\left(\frac{P_{Ed}/P_{Rd}}{M_{Ed}/M_{Rd}}\right) \quad (4)$$

The obtained numerical results were used to evaluate and assess the the applicability of the existing codifed provisions in Eurocode EC3, North American code of ANSI/AISC 360-16 as well as the newly developed design approach of CSM to cold-formed HSS IHexHS stub column specimens under combined compression and bending.

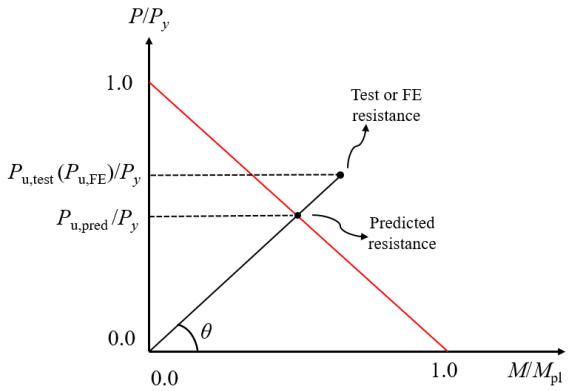

Fig. 9. Definition of on the load and moment interaction curve.

3. Assessment of design methods

3.1 General

In this section, the applicability of the design provisions set out in Eurocode 3 of EN 1993-1-12 (CEN 2007), ANSI/AISC 360-16 (AISC 2016) were examined for cold-formed HSS IHexHS stub columns under combined compression and bending using the numerical data generated in the parametric studies. In addition to the design codes, newly developed design approach of the Continuous Strength Method (CSM) was also evaluated with new end points determined in accordance with the design approach CSM. The interaction curve of the normalised axial compression and bending moment was updated using the design resistances from CSM for isolated loading condition of compression and bending and subsequently used to assess the accuracy and feasibility in the following sections. The obtained test results from the parametric studies were compared with the design codes and design approach with comparison of statistical results reported in Table 4 for cold-formed HSS IHexHS stub columns under combined compression and major and minor bending respectively. In Table 4, P_u is the ultimate load, P_{EC3}, P_{AISC} and P_{CSM} are the ultimate resistance predictions derived from EN 1993-1-12, ANSI/AISC 360-16 and design approach of CSM respectively. The ratio of the normalised axial load between FE results and the predicted cross-sectional resistance in compression was used to indicate the safety of the predictions. The normalised P_u/P_{pred} ratio greater than the unity indicate safe-sided predictions are provided.

3.2 European code EN 1993-1-12 (EC3)

The Eurocode EN 1993-1-1 specifies design provisons for conventional mild steel with grades up to S460. EN 1993-1-12 extend the scope of applicability of the design rules for conventional mild steels to high strength steels with grade above S460 up to S690, though the design provisions in EN 1993-1-12 extensively refer to the design framework and provisions in EN 1993-1-1. Hence, for cross-sections made up of conventional strength steel and high strength steel, same design rules are provided for cross-sections under combined compression and bending. EN 1993-1-1 codified linear interaction relationship betwee the compressive load and the bending moment for cross-sectional design under combined loading, as given in Eq. (5).

$$\frac{P_{Ed}}{P_{Rd}}+\frac{M_{Ed}}{M_{Rd}}\leq 1 \quad (5)$$

In the linear interaction equation, P_{Ed} and M_{Ed} are the design compressive load and design bending moment respectively. P_{Rd} and M_{Rd} are the design resistance according to the provisions codified in design codes. As per EN 1993-1-1, the design resistance of cross-sections classified as Class 1-3 are able to attain the yield load P_y, and the sections of Class 1-2 are able to achieve the plastic bending moment $M_{pl} = f_y W_{pl}$, whereas elastic bending moment $M_{el} = f_y W_{el}$ is used for Class 3 cross-sections, where W_{pl} and W_{el} are the plastic and elastic section modulus respectively. As the investigated specimens were carefully designed to be short enough to avoid any effect from global buckling, the interaction factor due to the second order effect was approximately equal to the unity and the amplified second order moment is negligible. Thus, the design bending moment was taken as the initial eccentricity value multiplied by the design compressive load. At present, no specifications for determination of cross-section classification of HSS IHexHS under bending are developed, thus the M_{pl} was used for the HSS IHexHS with maximum bending moment larger than the corresponding M_{pl} when the e_0/H and e_0/B are eight and six respectively. It was found that the compression resistance of the investigated specimens under such eccentricities were far lower than 2% of its yield load, leading to negligible effect to the bending moment capacity. The predicted ultimate resistances were compared with the FE results generated from parametric studies. The compressive resistance was normalised to the predicted compressive resistance and is plotted against the normalised ratio between design bending moment capacity and the plastic bending moment, as shown in Figs. 10–11. Fig 10 and Fig. 11 present the relationship between the normalised compression and normalised bending moment capacity about major axis and minor axis for cold-formed HSS IHexHS respectively with inclusion of EC3 interactive equation in Figs 10(b) –11(b). It is shown that EC3 design strengths are generally conservative, particularly for stocky sections, principally due to the conservative predictions of the end points of the design interaction curve. The end points of the EC3 interaction curve were derived without consideration of strain hardening and element interaction effect. In comparison with Q690 steel materials, specimens made from Q460 exhibit pronounced degree of conservatism for stockier sections as the increased level of strain hardening is associated with the stress-strain relationship of Q460 steel materials. As for Class 3 cross-sections, predictions from EC3 provide overly-conservative results indicating the current interaction design curve for IHexHS under combined compression and bending may be too optimistic. In particular, the increased level

of conservatism is proportional to the strength grades of the steel materials. The cold-formed HSS IHexHS made of Q460 is overly-predicted by EC3 in comparison with the counterparts made of Q690 steel as shown in Figs. 10–11 for combined compresion and both major axis and minor axis bending. Compared with the predictions for the specimens under combined compression and bending about major axis, less scattered predictions are obtained for sections under combined compression and bending about minor axis, though over-predicted resistances are still observed. The mean value of P_u/P_{EC3} are 1.21 and 1.28 for HSS IHexHS stub columns under combined compression and bending around major axis made of Q690 and Q460 materials with corresponding coefficients of variations (CoV) of 0.11 and 0.13 respectively. For HSS IHexHS stub columns under combined compression and bending around minor axis, relatively lower mean values of P_u/P_{EC3} were obtained which are 1.15 and 1.22 with the CoV of 0.03 and 0.07 for specimens comprising Q690 and Q460 materials.

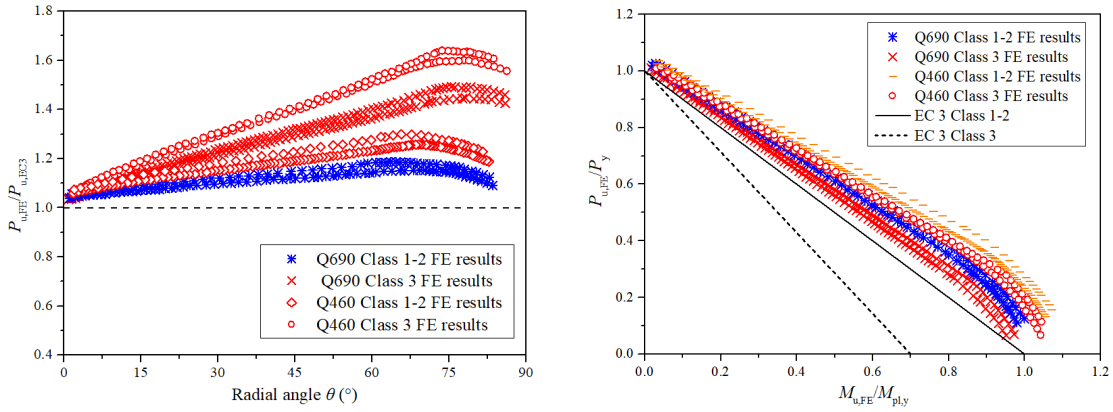

(a) (b)

Fig. 10. Comparison of the predicted cross-sectional resistance from EC3 for cold-formed HSS IHexHS under combined compression and major axis bending (a) Relationship between normalised ratio of ultimate load from FE to predictions from design code against radial angle (b) Interaction curve of normalised value of ultimate load to yield load against normalised bending moment.

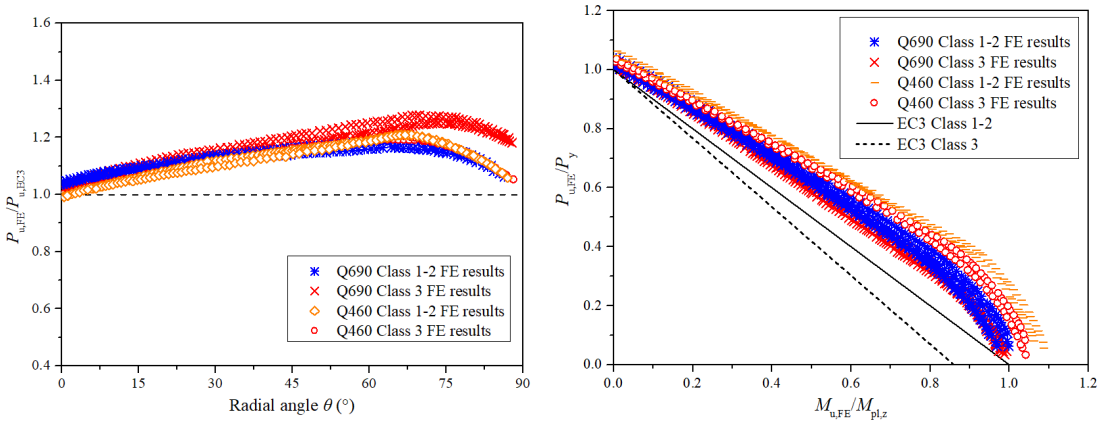

(a) (b)

Fig. 11. Comparison of the predicted cross-sectional resistance from EC3 for cold-formed HSS IHexHS under combined compression and minor axis bending (a) Relationship between normalised ratio of ultimate load from FE to predictions from design code against radial angle (b) Interaction curve of normalised value of ultimate load to yield load against normalised bending moment.

3.3 American specification ANSI/AISC 360-16 (AISC)

The North American design specification of ANSI/AISC 360-16 employ a pair of equations to design doubly symmetric cross-section structural components subject to combined compression and bending, as given in Eqs. (6)–(7).

$$\frac{P_{\mathrm{Ed}}}{P_{\mathrm{Rd}}}+\frac{8M_{\mathrm{Ed}}}{9M_{\mathrm{Rd}}}\le 1 \qquad \text{for } \frac{P_{\mathrm{Ed}}}{P_{\mathrm{Rd}}}\ge 0.2 \tag{6}$$

$$\frac{P_{\mathrm{Ed}}}{2P_{\mathrm{Rd}}}+\frac{M_{\mathrm{Ed}}}{M_{\mathrm{Rd}}}\le 1 \qquad \text{for } \frac{P_{\mathrm{Ed}}}{P_{\mathrm{Rd}}}<0.2 \tag{7}$$

For compact sections (equivalent to Class 1–2 sections in EC3), plastic bending moment M_{pl} can be formed and elastic bending moment M_{el} are designed for non-compact sections in AISC design provisions. The design moment is determied based on the end moment of the cross-sections multiplied by amplificaiton factor to account for the second order effect, which can be dervied in accordance with the Eq. (8), where P_{cr} is the elastic buckling load of the column. In present study, this amplication factor is approximately euqal to the unity.

$$\alpha_m = \frac{1}{1-\frac{P_{Ed}}{P_{cr}}} \quad (8)$$

The numerical results were also used to assess and evaluate the applicability of the design code of ANSI/ISC 360-16 to HSS IHexHS. As the investigated HSS IHexHS are not covered by ANSI/AISC 360-16, the estimation of the design bending moment follow the same approach employed in EN 1993-1-12. Comparison of the FE results with the predictions from ANSI/ISC 360-16 (strength-to-predicted strength) is plotted in Fig. 12 against the radial angle θ for HSS IHexHS under compression and major axis bending and the comparison of HSS IHexHS under compression and minor axis bending is shown in Fig. 13. In addition, the compression resistance is normalised to the yield load and design moment is normalised to the plastic moment capacity with interaction design curve added in Figs 12(b)–13(b). As can be seen from the figures and comparison results, the ultimate resistances were significantly under-estimated by AISC design curves. The mean value of P_u/P_{AISC} for Q690 and Q460 specimens are 1.16 and 1.22 with corresponding CoV of 0.10 and 0.13 respectively. In terms of the sections under compression and minor axis bending, the mean value of P_u/P_{AISC} for Q690 and Q460 specimens are 1.11 and 1.17 with the CoV of 0.05 and 0.07 respectively. Compared with the predictions from EC3, the ANSI/AISC 360-16 provides more consistent and accurate predictions.

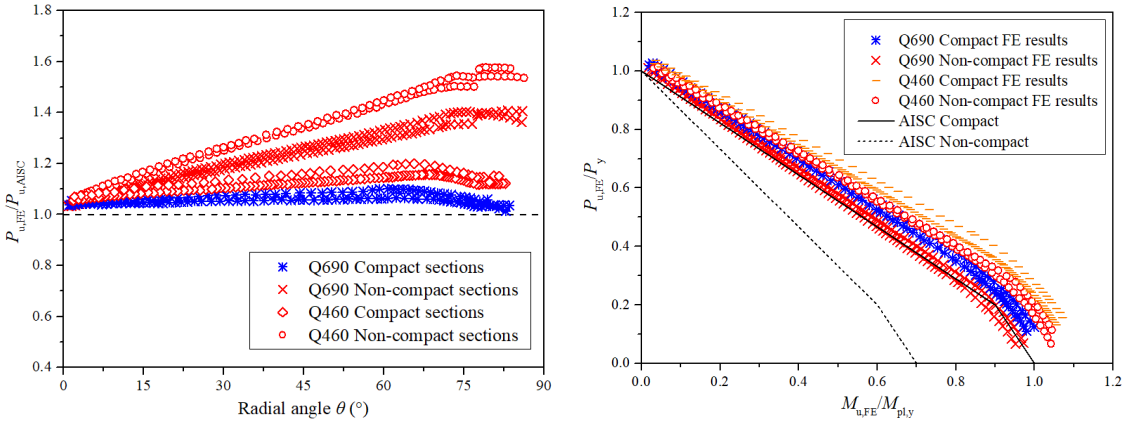

(a) (b)

Fig. 12. Comparison of the predicted cross-sectional resistance from AISC for cold-formed HSS IHexHS under combined compression and major axis bending (a) Relationship between normalised ratio of ultimate load from FE to predictions from design code against radial angle (b) Interaction curve of normalised value of ultimate load to yield load against normalised bending moment.

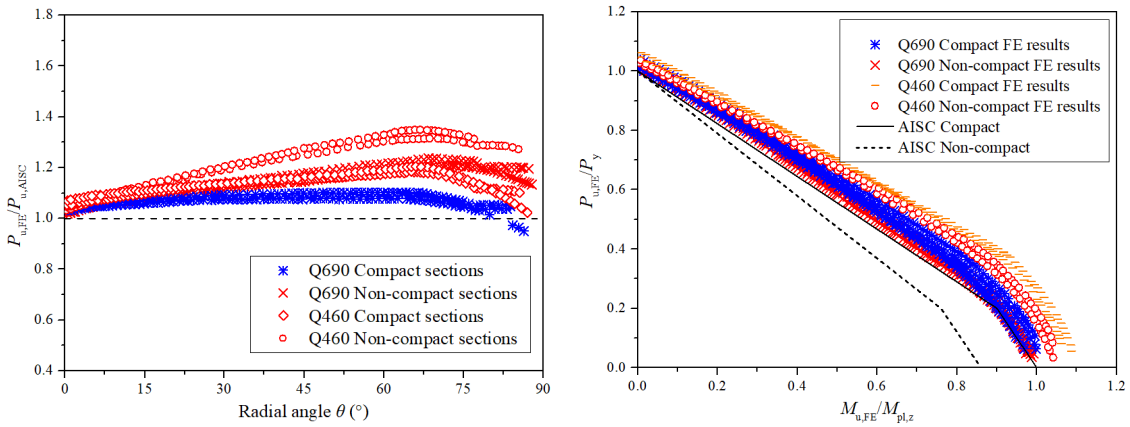

(a) (b)

Fig. 13. Comparison of the predicted cross-sectional resistance from AISC for cold-formed HSS IHexHS under combined compression and minor axis bending (a) Relationship between normalised ratio of ultimate load from FE to predictions from design code against radial angle (b) Interaction curve of normalised value of ultimate load to yield load against normalised bending moment.

3.4 Continuous Strength Method (CSM)

The Continuous Strength Method (CSM) is a deformation-based design method that can account for strain hardening and element interaction (Gardner 2008; Afshan and Gardner 2013). The employment of the CSM, relating the cross-sectional resistance to the deformation capacity, replace the traditional methodology of cross-section classification. The CSM is a systematic design approach which originally grounded up focusing on stainless steel (Afshan and Gardner 2013; Zhao et al. 2017) and is extended to the design of carbon steel sections for both hot-rolled sections and cold-formed sections (Yun et al. 2018; Yun and Gardner 2018). The observations of disparity and over-conservatism in cross-sectional resistance predictions from design codes underpin the necessities to improve the accuracy of the predictions using design approach of CSM. The design approach of CSM comprise two key components, (i) Base curve, which build a continuous relationship between the cross-sectional slenderness λ_p and deformation capacity (maximum attainable strain ε_{csm}) and (ii) CSM material model, which can explicitly capture the strain hardening of stress-strain curve. The design approach of CSM allows for the spread of plasticity and strain hardening, enabling the cross-section resistance particular for stocky sections to be considered explicitly. Hence, the CSM was used herein to generate more accurate end points anchored to the interaction curves, and the design equation of CSM for cold-formed HSS IHexHS under combined loading is proposed in a form analogous to EC3, given in Eq. (9).

$$\frac{P_{Ed}}{P_{csm,Rd}}+\frac{M_{Ed}}{M_{csm,Rd}}\leq 1 \quad (9)$$

The CSM have been developed and extended to be applicable for HSS tubular sections under pure compression (Lan et al. 2018) and pure bending (Lan et al. 2019). The base curve propsoed in Lan et al. (2018) for HSS tubular members was provided as follows in Eq. (10).

$$\frac{\varepsilon_{csm}}{\varepsilon_y}=\frac{0.294}{\lambda_p^{3.174}}\leq \min(15,\frac{C_1\varepsilon_u}{\varepsilon_y}) \quad \text{for } \lambda_p\leq 0.68 \quad (10)$$

where $\varepsilon_y = (f_y/E)$, and the constant C_1 is the material related coefficients.

Two upper bounds of 15 and $C_1\varepsilon_u/\varepsilon_y$ are proposed on the normalised cross-section deformation capacity ($\varepsilon_{csm}/\varepsilon_y$). The first limit of 15 is to avoid excessive plastic strain and subject to the material ductility requirement in EN 1993-1-1 (CEN 2005) and the second limit of $C_1\varepsilon_u/\varepsilon_y$ prevents over-prediction of material strengths. The material model, applicable for design approach of CSM, comprises quad-linear and bi-linear material model. The key characteristics of the stress-strain curves of Q460 steel materials comprise yield plateau and moderate level of strain hardening, which conform to the typical mode of quad-linear material model demonstrated in Fig. 14(a) and bi-linear model as shown in Fig. 14(b) was used to represent the relatively rounded response of Q690 steel material with no sharply defined yield point and plateau. To determine the CSM design stress of f_{csm}, strain hardening slope E_{sh} and the predicted strain ε_u corresponding to the ultimate stress are needed, as shown in Eq. (13). For quad-linear material model, the expressions given in Eq. (11) originally developed for hot-rolled steel by Yun and Gardner (2017) and bi-linear model employed in Yun and Gardner (2018) was used in this paper as shown in Eq. (12) for Q690 steel.

$$f_{csm}=\begin{cases} E_s\varepsilon_{csm} & \text{for } \varepsilon_{csm}\leq\varepsilon_y \\ f_y & \text{for } \varepsilon_y<\varepsilon_{csm}<\varepsilon_{sh} \\ f_y+E_{sh}(\varepsilon_{csm}-\varepsilon_{sh}) & \text{for } \varepsilon_{sh}<\varepsilon_{csm}<C_1\varepsilon_u \end{cases} \quad (11)$$

$$f_{csm}=f_y+E_{sh}(\varepsilon_{csm}-\varepsilon_{sh}) \quad \text{for } \varepsilon_y\leq\varepsilon_{csm} \quad (12)$$

$$E_{sh}=\frac{f_u-f_y}{C_2\varepsilon_u-\varepsilon_y} \quad (13)$$

where E_s is Young's modulus, f_y and f_u are the yield and ultimate tensile stress, ε_y and ε_u are the strains at the yield and ultimate stresses, respectively, ε_{sh} is the hardening strain defined as the end of the yield plateau after which the strain hardening initiates, $C_1\varepsilon_u$ represents the strain at the intersection point of the third stage of the model and the actual stress-strain curve. The other material coefficients C_2 is used to define the strain hardening modulus of E_{sh}. To determine the parameters of ε_u and ε_{sh}, and the coefficients of C_1 and C_2, the equations are summarised in Table 5 with considerations of normalised ratio between yield stress and ultimate stress proposed in Chen et al. (2022). The cross-section resistance predictions $P_{csm,Rd}$ from CSM under pure compression, was derived based on the gross cross-section area and the determination of the CSM design stress f_{csm}, as shown in Eq. (14).

$$P_{csm,Rd} = f_{csm} A \qquad \text{for } \lambda_p \le 0.68 \tag{14}$$

The determination of the bending resistance of a cross-section from CSM largely depends on whether the CSM strain has entered the range of strain hardening (i.e., $\varepsilon_{sh} < \varepsilon_{csm}$) or not. For steel materials with distinctive yield plateau, the CSM moment capacity can be calculated from Eqs. (15) – (16).

$$M_{csm} = M_{pl}\left[1-(1-\frac{W_{el}}{W_{pl}})/(\frac{\varepsilon_{csm}}{\varepsilon_y})^2\right] \qquad \text{for } \varepsilon_y < \varepsilon_{csm} \le \varepsilon_{sh} \tag{15}$$

$$M_{csm} = M_{pl}\left[1-(1-\frac{W_{el}}{W_{pl}})/(\frac{\varepsilon_{csm}}{\varepsilon_y})^2+0.1(\frac{\varepsilon_{csm}-\varepsilon_{sh}}{\varepsilon_y})\frac{E_{sh}}{E}\right] \qquad \text{for } \varepsilon_{csm} > \varepsilon_{sh} \tag{16}$$

With regard to the streel materials with typical rounded response, the CSM bending moment was determined from Eq. (17).

$$M_{csm} = M_{pl}\left[1+\frac{E_{sh}}{E}\frac{W_{el}}{W_{pl}}/(\frac{\varepsilon_{csm}}{\varepsilon_y}-1)-(1-\frac{W_{el}}{W_{pl}})/(\frac{\varepsilon_{csm}}{\varepsilon_y})^2\right] \qquad \text{for } \varepsilon_{csm} > \varepsilon_y \tag{17}$$

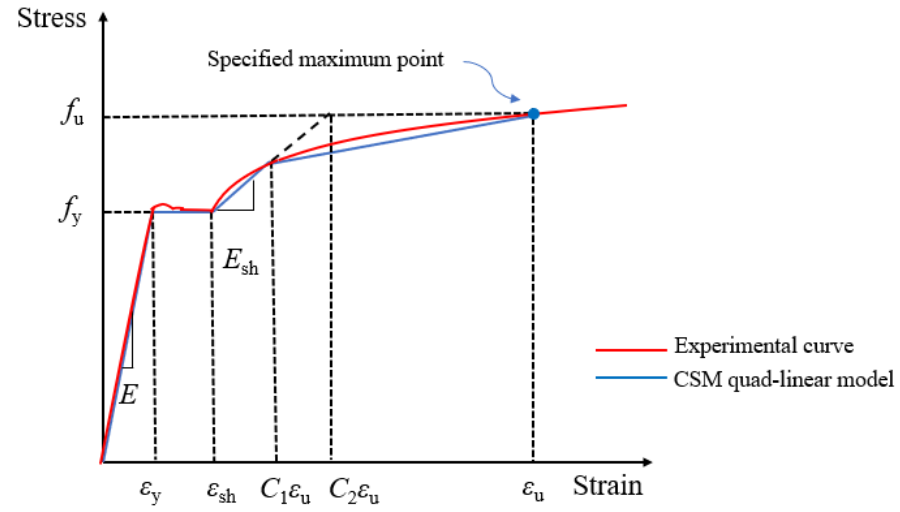

(a)

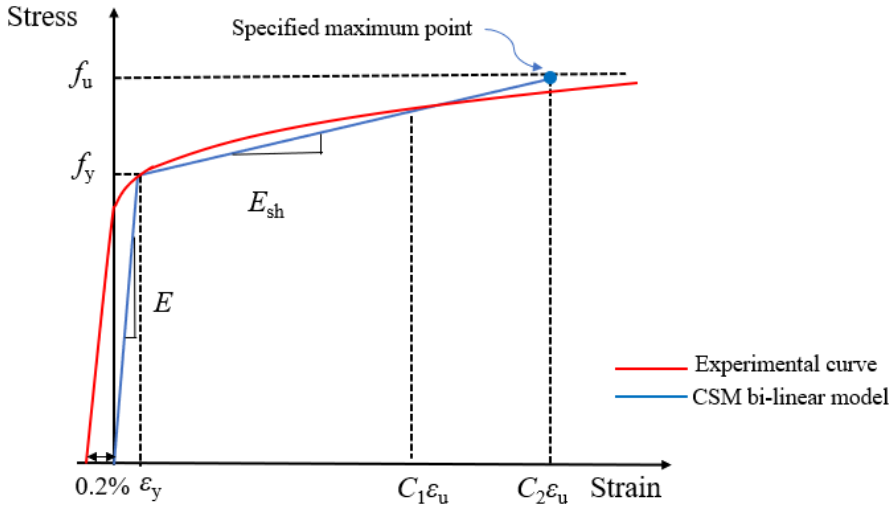

(b)

Fig. 14. Material model for design approach of CSM (a) Quad-linear material model for stress-strain curve with yield plateau and sharply defined yield point (b) Bi-linear material model for stress-strain with typically rounded response without yeild plateau.

Table 4 Comparison of FE results with predicted design resistances for HSS IHex stub columns under combined compression and bending.

Steel grade	Bending axis	No. of specimens	P_u/P_{EC3}		P_u/P_{AISC}		P_u/P_{CSM}	
			Mean	CoV	Mean	CoV	Mean	CoV
Q460	Major	450	1.28	0.13	1.22	0.13	1.10	0.04
Q690		450	1.21	0.11	1.16	0.10	1.06	0.04
Q460	Minor	450	1.22	0.07	1.17	0.07	1.12	0.05
Q690		450	1.15	0.06	1.11	0.05	1.08	0.03

The numerical results were used to assess the accuracy and the applicability of the proposed CSM method with updated end points anchored to the interaction curve. Comparisons of the FE results with the predictions from the proposed CSM (strength-to-predicted strength) are plotted in Fig. 15(a) against the radial angle θ for HSS IHexHS under compression and major axis bending amd in Fig. 16(a) for HSS IHexHS under compression and minor axis bending. The comparisons illustrate that the employment of the CSM leads to more consistent and less scatted resistance predictions compared with the design codes of EC3 and AISC. The mean P_u/P_{CSM} for cold-formed HSS IHexHS under major axis of Q690 and Q460 are 1.06 and 1.10 with corresponding CoVs of 0.04 and 0.04 respectively. The mean values of P_u/P_{CSM} for cold-formed HSS IHexHS under minor axis are also lower than the existing design codes with 1.08 and 1.12 for Q690 and Q460 steel materials with CoVs of 0.03 and 0.05 respectively. In addition, the interaction diagrams of normalised compression and normalised moment capacity are also plotted in Figs. 15(b) – 16(b) with notably improved accuracy in cross-section predictions. Nevertheless, Figs 15 – 16 generally reveal pronounced degree of conservatism as the applied loading varies from pure compression to pure bending for both design codes and proposed CSM interaction curve. Though more accurate and consistent predictions are obtained from CSM, predictions still exhibit conservatism for load combinations with lower axial ratios (larger radial angle). This can be principally attributed to two main issues, (i) the maximum deformation capacity was restricted to the strain of $15\varepsilon_y$ which impede the further exploitation of strain hardening, this restrictions can be relaxed based on certain case and (ii) the equations to derive the CSM bending moment was developed originally for SHS/RHS, the degree of plasticity formation and extent of strain hardening to which is different for IHexHS due to the effect of constituent plate element interaction from less onerous stress gradients.

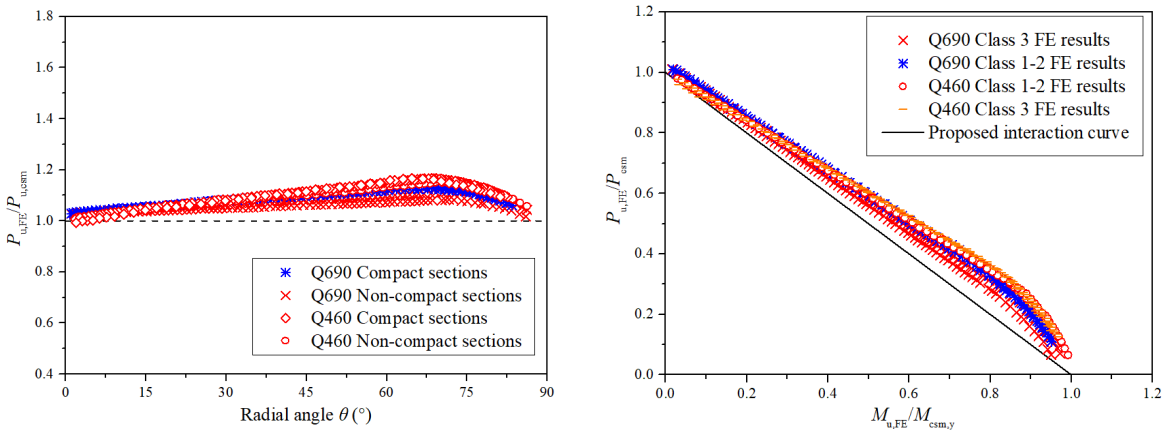

(a) (b)

Fig. 15. Comparison of the predicted cross-sectional resistance from design approach of CSM for cold-formed HSS IHexHS under combined compression and major axis bending (a) Relationship between normalised ratio of ultimate load from FE to predictions from design approach against radial angle (b) Interaction curve of normalised value of ultimate load to CSM predictions against normalised bending moment.

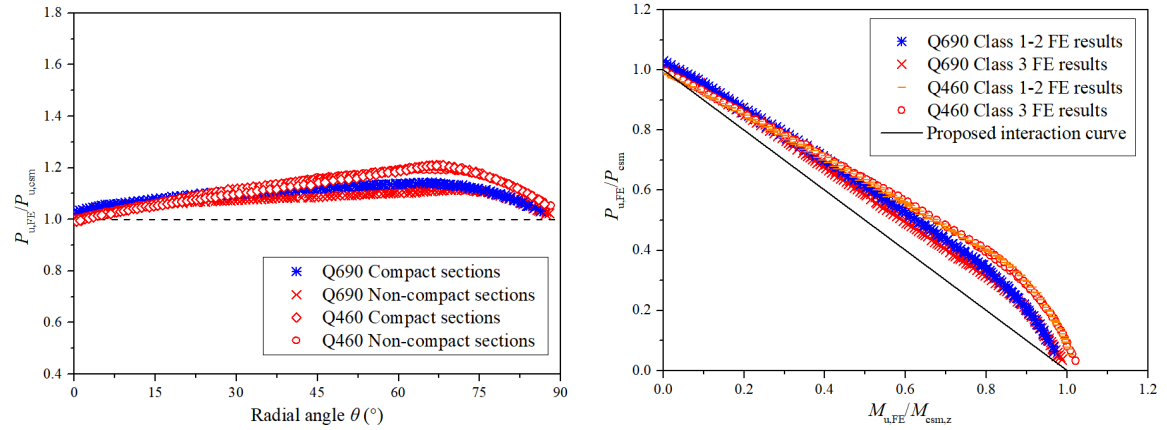

(a) (b)

Fig. 16. Comparison of the predicted cross-sectional resistance from design approach of CSM for cold-formed HSS IHexHS under combined compression and minor axis bending (a) Relationship between normalised ratio of ultimate load from FE to predictions from design approach against radial angle (b) Interaction curve of normalised value of ultimate load to CSM predictions against normalised bending moment.

Table 5 CSM material model for HSS materials.

	ε_u	ε_{sh}	C_1	C_2
$f_y/f_u \leqslant 0.85$	$0.6(1-\frac{f_y}{f_u})$	$0.1\frac{f_y}{f_u}-0.055$		
$0.85 < f_y/f_u \leqslant 0.9$	$0.8(1-\frac{f_y}{f_u})$	$-0.2\frac{f_y}{f_u}+0.2$	$\frac{\varepsilon_{sh}+0.3(\varepsilon_u-\varepsilon_{sh})}{\varepsilon_u}$	$\frac{\varepsilon_{sh}+0.55(\varepsilon_u-\varepsilon_{sh})}{\varepsilon_u}$
$0.9 < f_y/f_u$	$1-\frac{f_y}{f_u}$	0.02		

4. Reliability analysis

A reliability analysis was carried out to assess the reliability level and required partial factor for existing design methods and proposed CSM for cold-formed HSS IHexHS stub columns under combined loading. The first-order reliability analysis was performed in accordance with EN 1990 (CEN 2002) with key information briefly summarised herein. The material over-strength ratio $f_{y,mean}/f_{y,nom}$ = 1.15 and 1.10 was used for HSS Q690 and Q460 with CoVs of 0.045 and 0.035 respectively (Yun et al. 2022). The CoV of the geometric properties was taken as 0.05 (Afshan et al. 2015). The key reliability analysis results are shown in Table 6 and Table 7 for cold-formed HSS IHexHS stub columns under combined compression and major axis bending as well as combined compression and major axis bending. In table 6 and Table 7, b is the mean value correction factor, which can be derived based on least squares analysis between the resistance capacities from tests and design predictions from resistance model, where r_e is the experimental results and r_t is the theoretical results of the resistance model.

$$b = \frac{\sum r_e r_t}{\sum r_t^2} \tag{18}$$

V_δ is the CoV of the FE results relative to the resistance design model, which can be determined as follows, in Eqs. (19) – (21).

$$V_\delta = \sqrt{\exp(s_\Delta^{\,2}) - 1} \tag{19}$$

$$s_\Delta^{\,2} = \frac{1}{n-1}\sum_{i=1}^{n}(\Delta_i - \frac{1}{n}\sum_{i=1}^{n}\Delta_i)^2 \tag{20}$$

$$s_{\Delta}^{\ 2} = \ln(\delta_i) \tag{21}$$

where δ is the error term which is calculated for each pair data $\delta = r_e / br_t$.

The effect of the variability of the geometric and material in resistance function $g_{rt}(X)$ are accounted for through their coefficient of variation parameter V_{rt}. The calculation of this parameter is shown in Eq. (22)

$$V_{rt} = \frac{VAR\left[g_{rt}(\underline{X})\right]}{g_{rt}^{\ 2}(\underline{X}_m)} \cong \frac{1}{g_{rt}^{\ 2}(\underline{X}_m)} \times \sum_{i=1}^{j} \left(\frac{\partial g_{rt}}{\partial X_i}\sigma_i\right)^2 \tag{22}$$

V_r is the combined CoV incorporating both model and basic variable uncertainties, and γ_{M0} is the partial safety factor for cross section resistance. To determine the partial safety factor, design resistance value needs to be derived as follows,

$$r_d = b g_{rt}(\underline{X}_m)\exp(-k_{d,\infty}\alpha_{rt}Q_{rt} - k_{d,n}\alpha_{\delta}Q_{\delta} - 0.5Q^2) \tag{23}$$

where $\alpha_{rt} = Q_{rt}/Q$, $\alpha_{\delta} = Q_{\delta}/Q$, $Q_{rt} = \sqrt{\ln(V_{rt}^{\ 2}+1)}$, $Q_{\delta} = \sqrt{\ln(V_{\delta}^{\ 2}+1)}$, and $Q = \sqrt{\ln(V_r^{\ 2}+1)}$.

Based on the statistical results reported in Table 6 and Table 7, the design method of CSM provide partial factor γ_{M0} of 1.15, 1.16 for cold-formed HSS IHexHS stub columns made of Q690 and Q460 under combined compression and major bending, which were lower than the partial factor needed for design codes of EC3 and AISC. Similarly, the resultant partial factors for cold-formed HSS IHexHS stub columns made of Q690 and Q460 under combined compression and minor bending are 1.09 and 1.11 respectively, all lower than the required partial factor derived for EC3 and AISC. The average values of the ratio between the numerical resistances to predictions from CSM are significantly lower than the design codes of EC3 and AISC, resulting in improved accuracy in CSM resistance predictions. Furthermore, lower values of the V_{δ} were determined for CSM leading to notable improvement in cross-section predictions and increased consistency.

Table 6 Reliability analysis results for HSS IHexHS stub columns under combined compression and major axis bending.

Steel grade	Design method	No.	$k_{d.n}$	b	V_δ	V_r	γ_{Mo}
Q460	Eurocode 3	450	3.116	1.18	0.123	0.148	1.24
	AISC 360-16	450	3.116	1.15	0.119	0.145	1.26
	CSM	450	3.116	1.06	0.045	0.094	1.15
Q690	Eurocode 3	450	3.116	1.13	0.106	0.135	1.23
	AISC 360-16	450	3.116	1.12	0.122	0.147	1.30
	CSM	450	3.116	1.04	0.047	0.095	1.16

5. Conclusions

A comprehensive numerical investigation into the cross-section behaviour of the cold-formed HSS IHexHS stub columns under combined compression and bending has been conducted and presented in this paper. The finite element models were developed firstly and validated against the experimental results collated from previous investigations for cold-formed HSS SHS/RHS as well as cold-formed HSS OctHS. The validated FE models were subsequently used to conduct parametric studies covering a wider range of load combinations with a total of 1800 numerical models. The obtained numerical results were then used to assess the accuracy and applicability of the current design codes of EN 1993-1-1, EN 1993-1-12, and ANSI/AISC 360-16. It was shown that the existing design codes yield consistent but unduly conservative predictions, primarily due to the conservative predictions of the end points of the pure compression and pure bending in isolated loading conditions. Compared with the predictions obtained from the design codes, the design method of CSM provides improved accuracy in cross-section predictions in terms of both compression and bending, and end points with increased accuracy were anchored in the interaction curves. Based on the reliability analysis, design method of CSM provides more accurate, consistent and reliable predictions than the existing design codes with lower partial factors and statistical parameters. The design codes and the proposed design approach of CSM can be extended to cover the design of cold-formed HSS IHexHS under combined loading, despite the unduly conservative predictions from design codes, particular for stocky sections experiencing strain hardening.

Table 7 Reliability analysis results for HSS IHexHS stub columns under combined compression and minor axis bending.

Steel grade	Design method	No.	$k_{d.n}$	b	V_δ	V_r	γ_{Mo}
S460	Eurocode 3	450	3.116	1.15	0.075	0.112	1.12
	AISC 360-16	450	3.116	1.13	0.067	0.107	1.14
	CSM	450	3.116	1.11	0.062	0.103	1.11
S690	Eurocode 3	450	3.116	1.13	0.099	0.129	1.25
	AISC 360-16	450	3.116	1.08	0.053	0.098	1.15
	CSM	450	3.116	1.06	0.046	0.094	1.09

Data Availability Statement

Some or all data that support the findings of this study are available from the corresponding author upon reasonable request.

Acknowledgements

The research work presented in this paper was fully supported by a grant from the Research Grants Council of the Hong Kong Special Administrative Region, China (Project No. PolyU 15218918). The authors would also like to thank the support from Mr. Shuai Li and Mr. Jiachen Guo.

References

ABAQUS, Standard User's Manual, Version 6.14, Hibbitt, Karlsson and Sorensen, Inc., United States, 2014.

ANSI/AISC 360-16 (2016) Specification for Structural Steel Buildings.

AS 4100 (2020). Steel structures.

Afshan S, Francis P, Baddoo NR, and Gardner L (2015) Reliability analysis of structural stainless steel design provisions. *Journal of Constructional Steel Research* 114: 293-304.

Afshan S and Gardner L (2013) The continuous strength method for structural stainless steel design. *Thin-Walled Structures* 68: 42-49.

Chan T-M and Gardner L (2008) Compressive resistance of hot-rolled elliptical hollow sections. *Engineering Structures*

30(2): 522-532.

Chan T-M, Zhao XL and Young B (2015) Cross-section classification for cold-formed and built-up high strength carbon and stainless steel tubes under compression. *Journal of Constructional Steel Research* 106: 289-295.

Chen JB, Liu HX and Chan TM (2020) Material properties and residual stresses of cold-formed octagonal hollow sections. *Journal of Constructional Steel Research* 170.

Chen M-T and Young B (2019) Structural behavior of cold-formed steel semi-oval hollow section beams. *Engineering Structures* 185: 400-411.

Chen M-T and Young B (2020) Tests of Cold-Formed Steel Semi-Oval Hollow Section Members under Eccentric Axial Load. *Journal of Structural Engineering* 146(4).

Chen S, Fang H, Liu J-z and Chan T-M (2022) Design for local buckling behaviour of welded high strength steel I-sections under bending. *Thin-Walled Structures* 172: 108792.

EN 1990 (2002) Eurocode - Basis of structural design.

EN 1993-1-1 (2005) Eurocode 3: Design of Steel STRUCTURES – Part 1.1: General Rules and Rules for Buildings.

EN 1993-1-5 (2006) Eurocode 3: Design of Steel Structures – Part 1–5: Plated structural elements.

EN 1993-1-12 (2007) Eurocode 3: Design of Steel Structures – Part 1–12: Additional Rules for the Extension of EN 1993 up to Steel Grades S700.

Fang H, Chan T-M and Young B (2021) Experimental and Numerical Investigations of Octagonal High-Strength Steel Tubular Stub Columns under Combined Compression and Bending. *Journal of Structural Engineering* 147(1): 04020282.

Fang H, Chan T-M and Young B (2018) Material properties and residual stresses of octagonal high strength steel hollow sections. *Journal of Constructional Steel Research* 148: 479-490.

Gardner L (2008) The continuous strength method. *Proceedings of the Institution of Civil Engineers-Structures and Buildings* 161(3): 127-133.

Gardner L and Yun X (2018) Description of stress-strain curves for cold-formed steels. *Construction and Building Materials* 189: 527-538.

Lan XY, Chen JB, Chan T-M and Young B (2018) The continuous strength method for the design of high strength steel tubular sections in compression. *Engineering Structures* 162: 177-187.

Lan XY, Chen JB, Chan T-M and Young B (2019) The continuous strength method for the design of high strength steel tubular sections in bending. *Journal of Constructional Steel Research* 160: 499-509.

Liu JZ, Fang H, Chen S and Chan T-M (2022a) Material properties and residual stresses of high strength steel hexagonal

hollow sections. *Journal of Constructional Steel Research* 190: 107061.

Liu JZ, Fang H and Chan T-M (2022b) Investigations on material properties and residual stresses in cold-formed high strength steel irregular hexagonal hollow sections. *Thin-Walled Structures* 176: 109220.

Liu JZ, Fang H and Chan T-M (2022c) Experimental investigation on material properties and residual stresses in cold-formed high strength steel irregular octagonal hollow sections. *Journal of Constructional Steel Research* 191(107170): 107170.

Liu JZ, Fang H and Chan T-M (2022d) Experimental investigations on material properties and stub column behaviour of high strength steel irregular hexagonal hollow sections. *Journal of Constructional Steel Research* 196: 107343.

Liu JZ, Chen S and Chan T-M (2022e) Testing, numerical modelling and design of Q690 high strength steel welded T-section stub columns. *Engineering Structures* 259: 114142.

Liu JZ, Chen S and Chan T-M (2022f) Experimental and numerical investigations of hybrid high strength steel welded T-section stub columns with Q690 flange and Q460 web. *Thin-Walled Structures* 177: 109403.

Liu JZ, Fang H and Chan T-M (2022g) Experimental and numerical investigations on stub column behaviour of cold-formed high strength steel irregular octagonal hollow sections. *Thin-Walled Structures* 180: 109770.

Liu JZ, Fang H and Chan T-M (2022h) Structural behaviour of high strength steel hexagonal hollow section stub columns under axial compression. *Engineering Structures.* 268: 114653.

Liu JZ, Chen S and Chan T-M (2023) Hybrid welded T-section stub columns with Q690 flange and Q355 web: Testing, modelling and design. *Engineering Structures* 274: 115142

Ma J-L, Chan T-M and Young B (2015a) Material properties and residual stresses of cold-formed high strength steel hollow sections. *Journal of Constructional Steel Research* 109: 152-165.

Ma J-L, Chan T-M and Young B (2016) Experimental Investigation on Stub-Column Behavior of Cold-Formed High-Strength Steel Tubular Sections. *Journal of Structural Engineering* 142(5): 04015174.

Ma J-L, Chan T-M and Young B (2019) Cold-Formed High-Strength Steel Rectangular and Square Hollow Sections under Combined Compression and Bending. *Journal of Structural Engineering* 145(12).

Ma JL, Chan TM and Young B (2015b) Material properties and residual stresses of cold-formed high strength steel hollow sections. *Journal of Constructional Steel Research* 109: 152-165.

Yun X and Gardner L (2017) Stress-strain curves for hot-rolled steels. *Journal of Constructional Steel Research* 133: 36-46.

Yun X and Gardner L (2018) The continuous strength method for the design of cold-formed steel non-slender tubular

735 cross-sections. *Engineering Structures* 175: 549-564.
736 Yun X, Gardner L and Boissonnade N (2018) The continuous strength method for the design of hot-rolled steel cross-
737 sections. *Engineering Structures* 157: 179-191.
738 Yun X, Meng X and Gardner L (2022) Design of cold-formed steel SHS and RHS beam–columns considering the
739 influence of steel grade. *Thin-Walled Structures* 171: 108600.
740 Zhao O, Afshan S and Gardner L (2017) Structural response and continuous strength method design of slender stainless
741 steel cross-sections. *Engineering Structures* 140: 14-25.
742 Zhu JH and Young B (2011) Cold-Formed-Steel Oval Hollow Sections under Axial Compression. *Journal of Structural*
743 *Engineering* 137(7): 719-727.
744 Zhu JY, Chan T-M and Young B (2019) Cross-sectional capacity of octagonal tubular steel stub columns under uniaxial
745 compression. *Engineering Structures* 184: 480-494.